

RESEARCH ARTICLE

Electrochemical impedance spectroscopy unmasks high-risk atherosclerotic features in human coronary artery disease

Michael Chen¹  | Krit Suwannaphoom²  | Yas Sanaiha^{3,4}  | Yuan Luo⁵  |
Peyman Benharash^{3,4}  | Michael C. Fishbein²  | René R. Sevag Packard^{1,6,7,8,9,10,11,12} 

¹Division of Cardiology, Department of Medicine, David Geffen School of Medicine, University of California, Los Angeles, California, USA

²Department of Pathology and Laboratory Medicine, David Geffen School of Medicine, University of California, Los Angeles, California, USA

³Cardiovascular Outcomes Research Laboratories, University of California, Los Angeles, California, USA

⁴Division of Cardiac Surgery, Department of Surgery, David Geffen School of Medicine, University of California, Los Angeles, California, USA

⁵State Key Laboratory of Transducer Technology, Shanghai Institute of Microsystem and Information Technology, Chinese Academy of Sciences, Shanghai, People's Republic of China

⁶Ronald Reagan UCLA Medical Center, Los Angeles, California, USA

⁷West Los Angeles Veterans Affairs Medical Center, Los Angeles, California, USA

⁸Department of Physiology, David Geffen School of Medicine, University of California, Los Angeles, California, USA

⁹Department of Bioengineering, Henry Samueli School of Engineering and Applied Science, University of California, Los Angeles, California, USA

¹⁰Jonsson Comprehensive Cancer Center, University of California, Los Angeles, California, USA

¹¹Molecular Biology Institute, University of California, Los Angeles, California, USA

¹²California NanoSystems Institute, University of California, Los Angeles, California, USA

Correspondence

René R. Sevag Packard, Division of Cardiology, Department of Medicine, David Geffen School of Medicine, University of California, 10833 Le Conte Avenue, CHS Building Room 43-268, Los Angeles, CA 90095, USA.
Email: rpackard@mednet.ucla.edu

Funding information

U.S. Department of Veterans Affairs (VA), Grant/Award Number: BX004558; HHS | National Institutes of Health (NIH), Grant/Award Number: R56HL158569; UC | University of California, Los Angeles (UCLA)

Abstract

Coronary plaque rupture remains the prominent mechanism of myocardial infarction. Accurate identification of rupture-prone plaque may improve clinical management. This study assessed the discriminatory performance of electrochemical impedance spectroscopy (EIS) in human cardiac explants to detect high-risk atherosclerotic features that portend rupture risk. In this single-center, prospective study, $n = 26$ cardiac explants were collected for EIS interrogation of the three major coronary arteries. Vessels in which advancement of the EIS catheter without iatrogenic plaque disruption was rendered impossible were not assessed. $N = 61$ vessels underwent EIS measurement and histological analyses. Plaques were dichotomized according to previously established high rupture-risk

Abbreviations: ACS, adverse coronary syndrome; AUC, area under the curve; CAD, coronary artery disease; CI, confidence interval; CTA, computed tomography angiography; ECMO, extracorporeal membrane oxygenation; EIS, electrochemical impedance spectroscopy; FFR-CT, fractional flow reserve derived from CT; HPF, high-power field; ICA, invasive coronary angiography; IVUS, intravascular ultrasound; LAD, left anterior descending; LCx, left circumflex; Lp-PLA₂, lipoprotein-associated phospholipase A₂; LVIDd, left ventricular internal diameter at end-diastole; MI, myocardial infarction; MMP, matrix metalloproteinase; MPI, myocardial perfusion imaging; NC, necrotic core; NIRF, near-infrared fluorescence; NIRS, near-infrared spectroscopy; OCT, optical coherence tomography; OxNEFA, oxidized non-esterified fatty acids; RCA, right coronary artery; ROC, receiver operating characteristic; SMA, smooth muscle α -actin; SMC, smooth muscle cell; TCFA, thin-cap fibroatheroma.

parameter thresholds. Diagnostic performance was determined via receiver operating characteristic areas-under-the-curve (AUC). Necrotic cores were identified in $n = 19$ vessels (median area 1.53 mm^2) with a median fibrous cap thickness of $62 \mu\text{m}$. Impedance was significantly greater in plaques with necrotic core area $\geq 1.75 \text{ mm}^2$ versus $< 1.75 \text{ mm}^2$ ($19.8 \pm 4.4 \text{ k}\Omega$ vs. $7.2 \pm 1.0 \text{ k}\Omega$, $p = .019$), fibrous cap thickness $\leq 65 \mu\text{m}$ versus $> 65 \mu\text{m}$ ($19.1 \pm 3.5 \text{ k}\Omega$ vs. $6.5 \pm 0.9 \text{ k}\Omega$, $p = .004$), and ≥ 20 macrophages per 0.3 mm -diameter high-power field (HPF) versus < 20 macrophages per HPF ($19.8 \pm 4.1 \text{ k}\Omega$ vs. $10.2 \pm 0.9 \text{ k}\Omega$, $p = .002$). Impedance identified necrotic core area $\geq 1.75 \text{ mm}^2$, fibrous cap thickness $\leq 65 \mu\text{m}$, and ≥ 20 macrophages per HPF with AUCs of 0.889 (95% CI: 0.716–1.000) ($p = .013$), 0.852 (0.646–1.000) ($p = .025$), and 0.835 (0.577–1.000) ($p = .028$), respectively. Further, phase delay discriminated severe stenosis ($\geq 70\%$) with an AUC of 0.767 (0.573–0.962) ($p = .035$). EIS discriminates high-risk atherosclerotic features that portend plaque rupture in human coronary artery disease and may serve as a complementary modality for angiography-guided atherosclerosis evaluation.

KEYWORDS

electrochemical impedance spectroscopy, fibrous cap, high-risk plaque, human coronary artery disease, inflammation, invasive sensor, necrotic core

1 | INTRODUCTION

Coronary artery disease (CAD) remains a leading cause of mortality in the US and worldwide.¹ Particularly for patients who present with chest pain, appropriate CAD testing is critical for obviating adverse coronary syndrome (ACS). The decision to send a patient for imaging evaluation is based upon numerous factors, including the patient's risk-level, nature of angina pectoris, acuity of symptoms, and history of known CAD.²

CAD complications are often precipitated by plaque rupture leading to thrombus formation and ensuing myocardial ischemia and infarction.³ The understanding of the pathobiology of atherosclerosis has progressed significantly over the past decades. In particular, the presence of a large necrotic core overlain by a thin fibrous cap, positive remodeling, and spotty calcification, among others, are recognized as indicators of inflammatorily active, rupture-prone plaques.⁴ Despite contemporary strategies promoting aggressive reduction of cholesterol, triglyceride, and systemic inflammation levels, plaque rupture remains a prominent instigator of ACS.³ Accordingly, there is significant translational and clinical interest in the development of invasive and noninvasive imaging strategies to reveal pertinent components of atherosclerotic lesions prior to future clinical events.

Rapid, accurate identification of rupture-prone plaques would better inform subsequent steps for patient care and lead to improved outcomes.⁵ Noninvasive imaging

modalities such as coronary computed tomography angiography (CTA) provide comprehensive visualization of the entire coronary tree and elucidate the severity and extent of atherosclerotic plaques, an assessment that can be augmented and followed serially by fractional flow reserve derived from CT (FFR-CT).^{6,7} Cardiac nuclear imaging is a versatile modality that permits the assessment of specific plaque components or functional consequences of CAD, such as impaired myocardial blood flow and perfusion.^{8,9} However, noninvasive imaging modalities suffer from drawbacks, for example, blooming artifacts and the need for contrast agents in coronary CTA or reliance on radiotracers for myocardial perfusion imaging (MPI).

Invasive imaging modalities can inform CAD management via direct characterization of atherosclerotic lesions. Invasive coronary imaging should ideally elucidate both structural and compositional features of plaques. Electrochemical impedance spectroscopy (EIS) describes the resistive and charge-storing properties of biological tissue via measurement of the impedance—resistance to current flow—that arises in response to an applied alternating current (AC) across a range of frequencies.¹⁰ Our group previously demonstrated the differentiation of healthy arterial segments from lipid-laden atherosclerotic plaques¹¹ and the detection of pertinent compositional and morphological plaque features¹² using this strategy in animal models. In the present study, we assessed the discriminatory performance of EIS in human CAD from human cardiac explants to detect high-risk features known

to portend plaque rupture. Our results demonstrate that EIS uncovers high-risk plaque features in human CAD, thus enabling the distinction of apparently stable from rupture-prone lesions, with translational implications.

2 | METHODS

2.1 | Study population and workflow

The study population consisted of adult cardiac explants from patients undergoing orthotopic heart transplantation ($n=26$) (Figure S1) at the Ronald Reagan UCLA Medical Center from February 22, 2022, to December 9, 2022. Per IRB protocol, hearts were collected for EIS interrogation only when the attending pathologist was present. EIS measurements were performed in the three major coronary arteries ($n=61$): left anterior descending (LAD) ($n=21$), left circumflex (LCx) ($n=15$), and right coronary artery (RCA) ($n=25$). Vessels that were stented, severely stenosed, or totally occluded as to render impossible the advancement of the EIS catheter without iatrogenic vessel damage were excluded from interrogations; consequently, $n=17$ coronary arteries could not be interrogated. Upon completion of EIS measurements, the interrogated arteries were prepared for histological analyses as described below. This study was approved by the UCLA Office of the Human Research Protection Program Institutional Review Board.

2.2 | EIS sensor microfabrication

The EIS sensors were fabricated as previously described (Figure 1).¹³ Briefly, the sensors were composed of flexible polyimide strips (FPCexpress, Concord, ON, Canada) with copper pads ($600 \times 300 \mu\text{m}$) exposed at the distal end. The sensors were adhered to an inflatable balloon (Poba Medical, Flagstaff, AZ, USA) (15 mm in length, <1 mm diameter under deflation, and ~ 4.5 mm under inflation) affixed onto the distal end of the catheter tubing (25 cm in length) (Nordson Medical, Salem, NH, USA). Insulated copper wires were soldered onto the proximal contact pads of the flexible sensors to be connected to an impedance analyzer (Interface 1010E, Gamry Instruments, Warminster, PA, USA). Electroplating was performed in a solution of 0.5% w/v PtCl_4 at -0.6 V for 30 min to minimize contact impedance and improve EIS measurement specificity.

2.3 | EIS measurements

EIS was performed ex vivo by inserting the EIS catheter into the left or right coronary ostium and advancing the catheter to the target vessel site. Both prior and following catheter insertion, the target vessel was flushed with 70 mM NaCl solution using a 25-gauge needle. The balloon was inflated until contact was made with the endoluminal surface. Two replicates of all 15 pair-wise

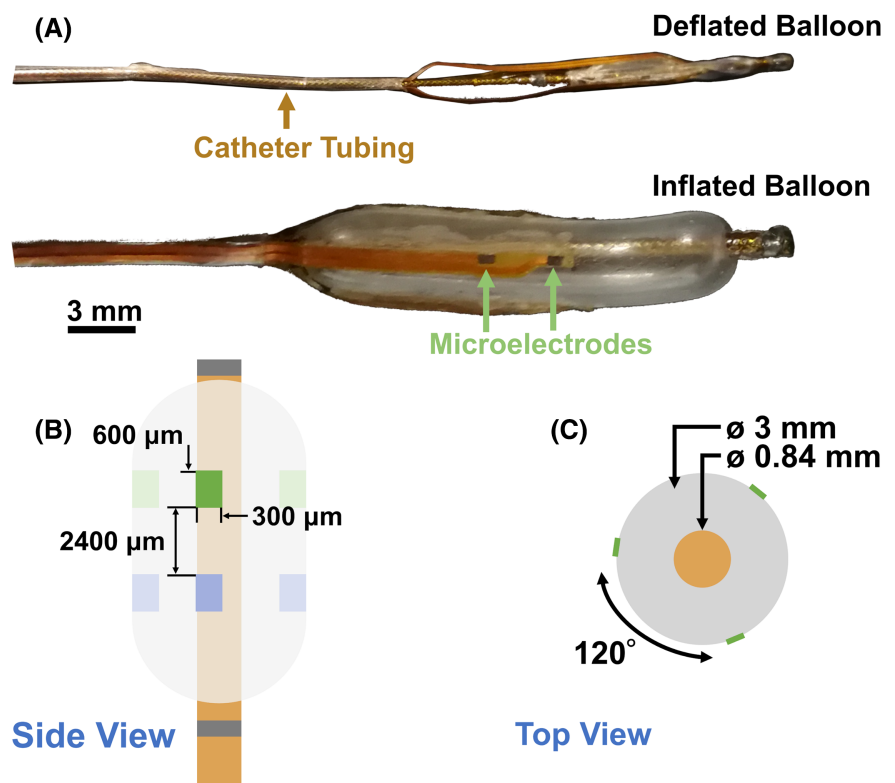


FIGURE 1 EIS balloon catheter design. (A) Zoomed-in photos of EIS balloon catheter design under deflation and inflation. (B) Side and (C) top-down views of the catheter schematics with dimensions.

permutations of EIS measurements were performed from 1 Hz to 1 MHz using AC signals with peak-to-peak voltages of 50 mV and five data points per decade. Impedance (Ω) and phase delay ($^\circ$)—the offset between input and output signals—were quantified. Prior to inflating the balloon, a set of measurements was also obtained with the balloon deflated to verify specificity of EIS signals. Analyses of EIS measurements were performed within the subrange of 10 Hz–100 kHz given that this constitutes the “plateau region” over which impedance values are stable, thus permitting accurate comparisons between measurements.¹¹ We performed background subtraction correction (BSC: inflated–deflated) for impedance and phase delay and selected maximal and minimal values, respectively, from each set of 15 permutations. Accordingly, the max impedance BSC and minimum phase delay BSC values were used for all analyses. During EIS measurements, the heart was kept gently wrapped in a damp towel. The distance relative to the ostium through which the catheter was advanced was recorded to ensure accurate marking of the location of the EIS sensors via sterile ink (MarginMarker, Vector Surgical, Waukesha, WI, USA).

2.4 | Histology

Following EIS interrogation, the coronary artery regions that were interrogated were marked in colored inks. The hearts were fixed in neutral-buffered formalin for ~24 h. The inked segments of coronary arteries were decalcified, if necessary, and cut at 2–3 mm intervals, corresponding to the sites of interrogation. Samples were then processed routinely, embedded in paraffin, sectioned, and stained with hematoxylin and eosin, Masson's trichrome, and Elastica-van Gieson (Statlab, McKinney, TX, USA) staining methods. Using the Leica Autostainer, Bond III system, and commercially available antisera, immunohistochemical staining was performed to detect vascular smooth muscle cell (SMC) (α -actin, Agilent Dako, Santa Clara, CA, USA), immune infiltrates (CD45, Agilent Dako, Santa Clara, CA, USA), macrophages (PU.1, Cell Marque, Rocklin, CA, USA), matrix metalloproteinase-9 (MMP-9, Abcam, Cambridge, MA, USA), and lipoprotein-associated phospholipase A₂ (Lp-PLA₂, OriGene, Rockville, MD, USA). Appropriate positive and negative control tissues were also stained. Atherosclerotic plaques were analyzed for % stenosis, intimal/medial thickness ratio, necrotic core area, necrotic core arc, fibrous cap thickness, SMC infiltration, immune cell infiltration, macrophage infiltration, and MMP-9 and Lp-PLA₂ expression. Percent stenosis was defined as the ratio of the neointimal area

to the total area bound by the internal elastic lamina. The mean thicknesses of the intimal and medial layers were calculated by averaging the thicknesses of the respective layers measured at four locations equidistant from each other along the internal and external elastic laminae. The intima/media thickness ratio was defined as the ratio of the average intimal thickness to the average medial thickness. Percent SMC, % immune infiltration, and MMP-9 and Lp-PLA₂ expression were obtained by calculating the percent intimal area that displayed positive α -actin, CD45, MMP-9, or Lp-PLA₂ staining, respectively. Macrophage infiltration was defined as the number of PU.1-positive nuclei within the neointima. The transcription factor PU.1 is expressed at high levels by macrophages and interacts with myriad regulatory factors such as GATA-2¹⁴ and SWI/SNF¹⁵ to regulate PU.1-dependent leukocyte lineage differentiation. Visual analyses of corresponding H&E slides were conducted to verify that PU.1-stained cells possessed the appropriate morphological features of macrophages. Necrotic core area was obtained by summing the individual areas of all identified necrotic cores. The % intimal area occupied by necrotic cores was calculated as the ratio of the total area of the necrotic core to the neointimal area. Necrotic core arc was obtained by dividing the total length of the necrotic core edges closest to the lumen by the circumference of the internal elastic lamina. The fibrous cap thickness was measured at the thinnest section of the fibrous cap. Necrotic core area and fibrous cap thickness data were stratified by high-risk thresholds— $\geq 1.75 \text{ mm}^2$ and $\leq 65 \mu\text{m}$ for necrotic core area^{16–18} and fibrous cap thickness,¹⁸ respectively—established by previous studies. All analyses were conducted by two experienced pathologists blinded to patient characteristics (K.S. and M.C.F.).

2.5 | Statistics

Results are presented as mean \pm SEM, median (1st quartile–3rd quartile), or n (%). Mann–Whitney U -test was performed to evaluate differences in EIS impedance and phase delay values between vessels with higher- and lower-risk plaque characteristics. Receiver operating characteristic (ROC) analyses were performed to assess the diagnostic performance of EIS impedance and phase delay for the identification of high-risk plaque features. Generalized estimating equations with robust variance estimation were utilized to adjust for clustering effects from within-patient variability. Youden's index was calculated as [sensitivity + specificity – 1]. Stata v17 (StataCorp., College Station, TX, USA), SPSS v26 (IBM, Armonk, NY, USA), and Prism v9 (GraphPad, Boston,

MA, USA) were used for statistical analyses. A *p*-value <.05 was considered significant.

3 | RESULTS

3.1 | Patient characteristics

Study patients had a mean age of 50.1 ± 2.7 years, were 73% male, and a majority presented with non-ischemic cardiomyopathy (73%) (Table 1). *N*=7 patients had previously undergone coronary revascularization procedures. *N*=3 patients had a history of myocardial infarction (MI). Mean left ventricular internal diameter at end-diastole (LVIDd) and ejection fraction prior to transplant were 6.1 ± 0.3 cm and $27.2 \pm 3.1\%$, respectively. A majority (62%) of patients had concomitant moderate–severe valvular regurgitation. Similarly, 62% of patients were on mechanical support (*n*=9 Impella and *n*=3 intra-aortic balloon pump) or extracorporeal membrane oxygenation (ECMO) (*n*=4) prior to transplant. 39% and 27% of patients had a history of atrial fibrillation or ventricular tachycardia, respectively.

3.2 | Histology

Histological parameters of analyzed human coronary arteries are presented in Table 2. All arteries exhibited luminal narrowing; the minimum % stenosis was 11% and the median % stenosis across all arteries was 45% (33%–66%). Necrotic cores were present in *n*=19 arteries (*n*=8 from patients with ischemic cardiomyopathy, *n*=11 from patients with non-ischemic cardiomyopathy); the median area, % intimal area occupied by necrotic core, and arc were 1.53 mm^2 ($0.87\text{--}2.64 \text{ mm}^2$), 26% (17%–45%), and 118° ($89^\circ\text{--}160^\circ$), respectively. Median fibrous cap thickness was $62 \mu\text{m}$ (19–158 μm). Calcification was identified only in arteries that also harbored a necrotic core (*n*=15) and often overlapped with the necrotic core (Figure 2, bottom row). Median calcified area, %intimal area occupied by calcification, and arc were 0.48 mm^2 ($0.23\text{--}1.35 \text{ mm}^2$), 8% (5%–33%), and 43° ($34^\circ\text{--}77^\circ$), respectively.

Although only 42% of arteries possessing a necrotic core displayed a necrotic core area $\geq 1.75 \text{ mm}^2$, all such arteries exhibited $\geq 50\%$ luminal narrowing, with equal numbers in the 50%–69% and $\geq 70\%$ categories (Figure 3). Among arteries with necrotic core area $\geq 1.75 \text{ mm}^2$, no significant differences in necrotic core area (3.32 mm^2 vs. 3.14 mm^2 , *p*=.886) were observed between arteries with $\geq 70\%$ stenosis and those 50%–69% stenosis. Large necrotic cores were discovered in arteries from both ischemic and non-ischemic cardiomyopathy patients in equal numbers. In contrast, arteries with necrotic core area $< 1.75 \text{ mm}^2$

TABLE 1 Patient characteristics.

Patient characteristics	
Age, years	50.1 ± 2.7
Gender, male	19 (73)
Ethnicity	
African American	2 (7)
Asian American	4 (15)
Hispanic	10 (39)
Non-Hispanic White	10 (39)
Cardiomyopathy	
Ischemic	7 (27)
Non-ischemic	19 (73)
Echocardiography	
LVIDd (cm)	6.1 ± 0.3
Ejection fraction (%)	27.2 ± 3.1
Valvular abnormalities	16 (62)
Arrhythmias	
Atrial fibrillation	10 (39)
Ventricular tachycardia	7 (27)
Mechanical support	
Impella	9 (35)
Intra-aortic balloon pump	3 (12)
ECMO	4 (15)
Risk factors	
Hypertension	11 (42)
Dyslipidemia	13 (50)
Diabetes	7 (27)
BMI, kg/m ²	26.2 ± 0.8
Tobacco use	
Former	4 (15)
Never	22 (85)
Family history of CAD	9 (35)
Laboratory results	
Sodium (mmol/L)	135.7 ± 0.8
Creatinine ($\mu\text{mol/L}$)	106.1 ± 8.8
GFR (mL/min/1.73 m ²)	
≥ 90	11 (42)
< 90	54.1 ± 3.3
Glucose (mmol/L)	6.4 ± 0.3
HbA1c (%)	5.7 ± 0.1
Albumin (g/L)	39.2 ± 0.9
Total cholesterol (mmol/L)	3.5 ± 0.1
LDL cholesterol (mmol/L)	1.7 ± 0.1
HDL cholesterol (mmol/L)	1.2 ± 0.1
Triglycerides (mmol/L)	1.2 ± 0.1

Note: Values are presented as mean \pm SEM or *n* (%).

Abbreviations: BMI, body mass index; CAD, coronary artery disease; ECMO, extracorporeal membrane oxygenation; GFR, glomerular filtration rate; HbA1c, hemoglobin A1C; HDL, high-density lipoprotein; LDL, low-density lipoprotein; LVIDd, left ventricular internal diameter end-diastole.

exhibited a greater range of luminal narrowing. Approximately, half of the arteries with a fibrous cap (53%) possessed a fibrous cap $\leq 65\mu\text{m}$ in thickness. Arteries with fibrous cap $\leq 65\mu\text{m}$ exhibited stenoses ranging from 25% to $\geq 70\%$, while arteries with fibrous cap $>65\mu\text{m}$ exhibited

TABLE 2 Histological analysis of coronary lesions.

Stenosis (%)	45	(33–66)
0–24	9	(15)
25–49	27	(44)
50–69	13	(21)
≥ 70	12	(20)
Intimal/medial thickness ratio	1.46	(0.85–2.91)
SMA ⁺ area (mm ²)	0.55	(0.29–0.88)
PU.1 ⁺ nuclei (<i>n</i>)	90	(21–509)
CD45 ⁺ area (mm ²)	0.01	(0.01–0.02)
Necrotic core		
Total area (mm ²)	1.53	(0.87–2.64)
% Intimal area	26	(17–45)
Arc (°)	118	(89–160)
Fibrous cap		
Minimum thickness (μm)	62	(19–158)

Note: The presented parameters are circumscribed to the neointima. Stenosis categories are presented as *n* (%); all other parameters are presented as median (Q1–Q3).

Abbreviation: SMA, smooth muscle α -actin.

stenoses $\geq 50\%$ only. Among arteries with fibrous cap $\leq 65\mu\text{m}$, no significant differences were found for fibrous cap thickness among the stenosis categories ($p = .321$). A majority of thin fibrous caps (80%) were from arteries of non-ischemic cardiomyopathy patients. Additionally, 75% of arteries with large necrotic cores possessed thin fibrous caps. Among the arteries with large necrotic cores but a fibrous cap thicker than the $65\mu\text{m}$ threshold, half exhibited a fibrous cap thickness very close to the $65\mu\text{m}$ threshold.

Representative examples of coronary arteries with mild, moderate, and severe disease are presented in [Figure 2](#).

3.3 | EIS

Human coronary artery EIS profiles varied according to underlying atherosclerosis features ([Figure 4](#)). Arteries with no necrotic core exhibited lower impedance ([Figure 4A,B](#)) throughout the endoluminal surface. In contrast, arteries with necrotic cores displayed endoluminal non-uniformity characterized by localized high impedance measures ([Figure 4C–F](#)). The focal increases in impedance ([Figure 4D,F](#)) demonstrate the spatial specificity of EIS to detect pertinent atherosclerotic plaque components ([Figure 4C,E](#)). Larger necrotic cores indicate increased lipid content and acellular area. Both factors decrease the overall electrical conductivity and thus increase

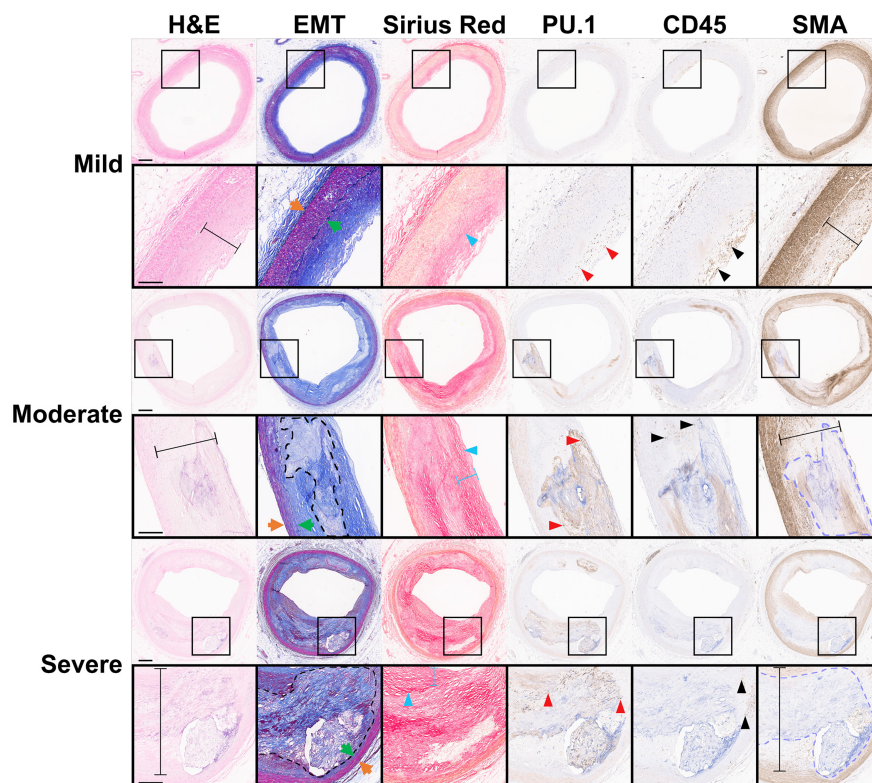


FIGURE 2 Histological sections of coronary arteries. Examples of mild (top), moderate (middle), and severe (bottom) necrotic core burden are presented. Black bars delineate the neointima. Fibrous cap is indicated by cyan bars. Green and orange arrows denote the internal and external elastic laminae, respectively. Cyan, red, and black arrowheads indicate positive staining for collagen (Sirius Red), macrophages (PU.1), and leukocytes (CD45), respectively. The black and purple dashed lines outline the necrotic core and calcification, respectively. Scale bars are $500\mu\text{m}$ (zoomed out) and $200\mu\text{m}$ (inset). EMT, elastic Masson's trichrome; H&E, hematoxylin & eosin; SMA, smooth muscle α -actin.

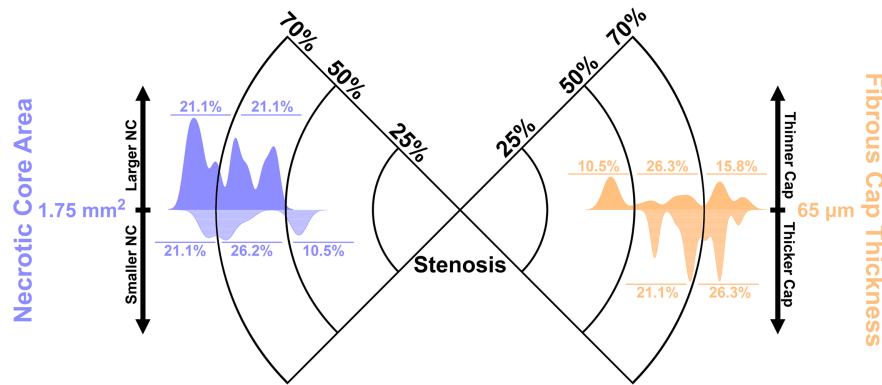


FIGURE 3 Distribution of coronary high-risk atherosclerotic features stratified by stenosis burden. Histogram depiction of necrotic core (NC) area (left, purple) and fibrous cap thickness (right, orange) by %stenosis category (0%–24%, 25%–49%, 50%–69%, ≥70%; radial distance from center) and according to the threshold (upward vertical axis, darker shade) indicating increased susceptibility to rupture. Vessels that do not exhibit high-risk features (i.e. those with necrotic core area $<1.75 \text{ mm}^2$ or fibrous cap thickness $>65 \mu\text{m}$) are represented by the downward histograms (downward vertical axis, lighter shade). The height of each peak represents the magnitude of the corresponding plaque parameter (e.g., a taller purple peak represents a larger necrotic core). The numbers above and below the graphs indicate the proportion of vessels within a given stenosis category and above or below the high-risk threshold.

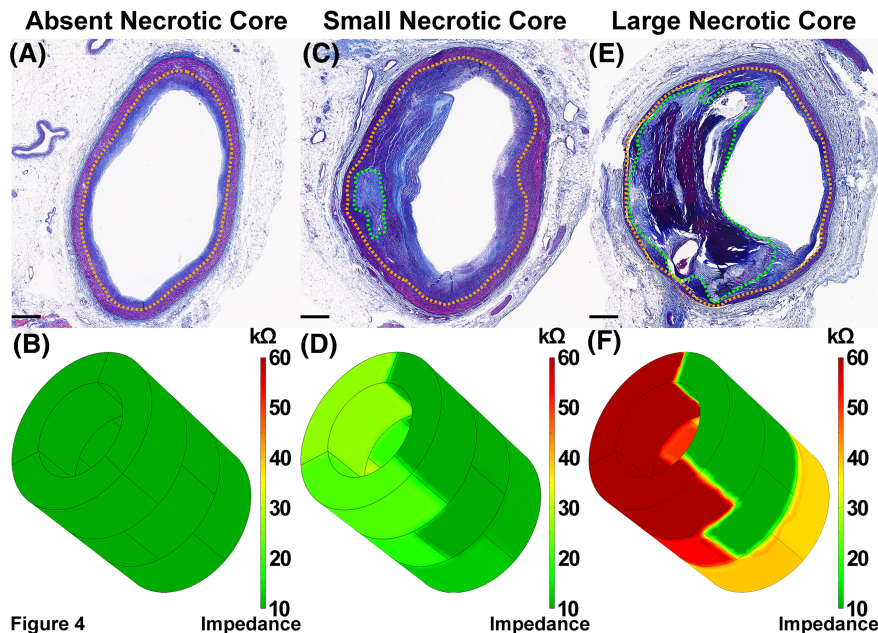


FIGURE 4 3D EIS mapping of endoluminal surface captures eccentricity of atherosclerosis and identifies pertinent plaque features. The six-point electrochemical impedance spectroscopy (EIS) sensor configuration permits 360° interrogation of the endoluminal surface to precisely capture atherosclerosis eccentricity. Representative examples of coronary arteries with (A, B) no necrotic core, (C, D) small ($<1.75 \text{ mm}^2$) necrotic core, and (E, F) large ($\geq 1.75 \text{ mm}^2$) necrotic core are presented. Advanced lesions displayed large necrotic cores that were in part calcified (dark purple), such as the example presented in (E). Larger necrotic cores manifest as increased impedance. Green and orange dotted lines delineate the necrotic core and internal elastic lamina, respectively. Scale bars are $500 \mu\text{m}$.

arterial impedance. Consequently, atherosclerotic lesions with larger necrotic core size present with increased impedance (Figure 4C,D vs. E,F).

In addition, we performed ROC analyses across the “plateau region”¹¹—the AC frequencies over which impedance values are stable (10 Hz–100 kHz)—to determine the impedance and phase delay values above

which plaque characteristics that portend rupture susceptibility¹⁹ may be identified. Mean impedance for arteries with necrotic core area $\geq 1.75 \text{ mm}^2$ was significantly elevated compared with arteries with necrotic core area $<1.75 \text{ mm}^2$ ($19.8 \pm 4.4 \text{ k}\Omega$ vs. $7.2 \pm 1.0 \text{ k}\Omega$, $p = .019$) (Figure 5A). Similarly, arteries with fibrous cap thickness $\leq 65 \mu\text{m}$ demonstrated higher mean impedance than

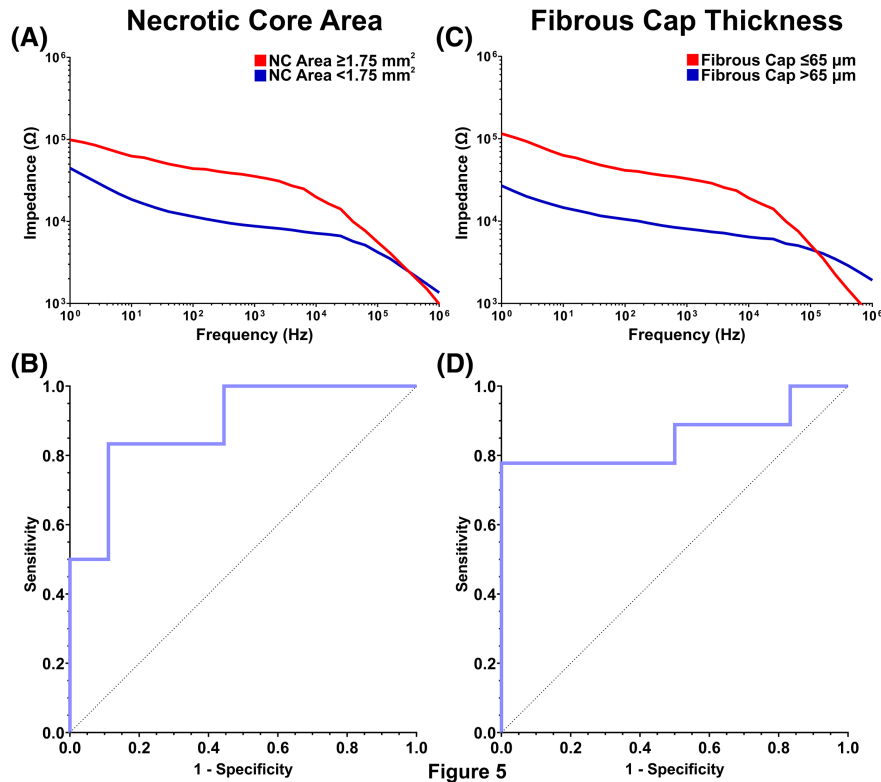


FIGURE 5 EIS impedance profiles with ROC analyses of coronary atherosclerotic characteristics that portend increased susceptibility to rupture. (A, C) Representative electrochemical impedance spectroscopy (EIS) impedance profiles of vessels with (red) or without (blue) high-risk plaque features, as well as (B, D) ROC analyses depicting the ability of impedance to identify plaque features that exceed the high-risk threshold, are presented for (A, B) necrotic core (NC) area and (C, D) fibrous cap thickness.

arteries with fibrous cap thickness $>65\ \mu\text{m}$ ($19.1 \pm 3.5\ \text{k}\Omega$ vs. $6.5 \pm 0.9\ \text{k}\Omega$, $p = .004$) (Figure 5C), and arteries with ≥ 20 macrophages per 0.3 mm-diameter high-power field (HPF) displayed elevated mean impedance compared with arteries with < 20 macrophages per HPF ($19.8 \pm 4.1\ \text{k}\Omega$ vs. $10.2 \pm 0.9\ \text{k}\Omega$, $p = .002$) (Figure S2A). Accordingly, impedance increases with a larger necrotic core, a thinner minimum fibrous cap thickness, and/or increased neointimal macrophage infiltration. Severely stenosed ($\geq 70\%$) arteries exhibited phase delay values of lower magnitude compared with less stenosed ($< 70\%$) arteries (Figure S3A). Both impedance and phase delay discriminated higher risk from lower risk plaque features. Impedance identified necrotic core area $\geq 1.75\ \text{mm}^2$, fibrous cap thickness $\leq 65\ \mu\text{m}$, and elevated macrophage infiltration with AUCs of 0.889 (95% CI: 0.716–1.000) ($p = .013$) (Figure 5B), 0.852 (0.646–1.000) ($p = .025$) (Figure 5D), and 0.835 (0.577–1.000) ($p = .028$) (Figure S2B), respectively. Phase delay discriminated arteries with $\geq 70\%$ stenosis with an AUC of 0.767 (0.573–0.962) ($p = .035$) (Figure S3B). An impedance of $\geq 8975\ \Omega$ separated necrotic cores with areas $\geq 1.75\ \text{mm}^2$ from smaller necrotic cores with sensitivity, specificity, and Youden's index of 0.833, 0.889, and 0.722, respectively; fibrous cap thickness $\leq 65\ \mu\text{m}$ from thicker caps with sensitivity, specificity, and Youden's index of 0.778, 1.000, and 0.778, respectively; and heightened macrophage infiltration with sensitivity, specificity, and Youden's index of 0.750, 0.976, and 0.726, respectively. For ease of applicability in subsequent validation studies, we propose $\geq 9000\ \Omega$

as the threshold for identification of high-risk plaque features portending rupture risk. Phase delay $\geq -13^\circ$ (i.e., less negative) distinguished arteries with stenosis $\geq 70\%$ from less stenosed arteries with a sensitivity, specificity, and Youden's index of 1.000, 0.750, and 0.750 respectively.

We further investigated the association of impedance with known markers of plaque progression and instability. Impedance exhibits positive, moderate correlations with both MMP-9 ($r = .771$, $p < .001$) (Figure S4A) and Lp-PLA2 ($r = .636$, $p < .001$) (Figure S5A). Stratification of MMP-9 and Lp-PLA2 expression levels by our proposed impedance threshold of $\geq 9000\ \Omega$ further confirms increased levels of MMP-9 ($0.410 \pm 0.107\%$ vs. $0.162 \pm 0.046\%$, $p = .040$) (Figure S4B) and Lp-PLA2 ($0.131 \pm 0.016\%$ vs. $0.055 \pm 0.011\%$, $p < .001$) (Figure S5B) for vessels exhibiting impedance $\geq 9000\ \Omega$. We present representative examples of MMP-9 (Figure S4C,D) and Lp-PLA2 (Figure S5C,D) expression in coronary arteries.

4 | DISCUSSION

CAD complications remain a prominent cause of acute coronary syndromes. Early-stage detection of rupture-prone lesions would improve clinical outcomes by forestalling acute thrombus formation and potential downstream ischemia. A wealth of literature has revealed and validated key plaque features, such as a large necrotic core and a thin fibrous cap, which indicate

increased susceptibility to rupture. In the present study, we demonstrate the ability of EIS, via impedance, to differentiate large necrotic cores, thin fibrous caps, and elevated neointimal macrophage infiltration, atherosclerotic plaque features that portend future risk of rupture, and via phase delay, identify severe luminal stenosis, thus demonstrating the potential for EIS to provide comprehensive invasive plaque assessment in humans.

Previous studies have demonstrated the capability of EIS to distinguish atherosclerotic from healthy tissue via frequency-dependent electrical impedance.¹⁰ Initial studies deployed a four-electrode linear configuration to compare *ex vivo* impedance readings of healthy and diseased rabbit arteries.¹⁰ Our group introduced a design with reduced dimensions featuring two distinct electrodes forming one sensor pair.¹¹ The smaller dimensions improved spatial specificity and contact with uneven endoluminal topography, while the enlarged separation of electrodes augmented signal-to-noise ratio and provided deeper tissue penetration of signals.¹¹ However, the focal nature of these designs does not capture the heterogeneity of atherosclerosis; physical rotation of sensors between individual measurements would be required to account for plaque eccentricity. Catheter rotation during balloon inflation risks iatrogenic plaque disruption or vessel wall injury; under balloon deflation, placement of the sensors might be altered by rotation, thus hampering accurate atherosclerotic assessment at that vessel segment. The circumferential 6-point design¹³ utilized in the present study improves spatial specificity by providing more granular measurements with 120° angular resolution and facilitates uninterrupted 360° interrogation of a vessel segment. We previously illustrated the utility of EIS for holistic atherosclerotic characterization in a rabbit atherosclerosis model.¹² The present study in human CAD demonstrates EIS discrimination of high-risk atherosclerosis features via an impedance threshold that identifies rupture-prone lesions.

Several plaque features that indicate a susceptibility to rupture have been identified, most prominently a large necrotic core size^{16–18} and thin fibrous cap.²⁰ Histological analyses of culprit lesions have revealed the greater risk that accompanies a larger necrotic core.^{16–18} In a study of >200 cases of sudden coronary death, Virmani et al. demonstrated an increase in necrotic core size from stable fibrous cap atheroma, to thin-cap fibroatheroma (TCFA), to ruptured plaques, with a mean necrotic core size of 1.7 mm² in TCFA.¹⁸ In a similar assessment of coronary lesions also from sudden coronary death patients, Kolodgie et al. discovered a mean necrotic core size of 1.95 mm² among TCFA.¹⁷ Cheruvu et al. identified a somewhat smaller average necrotic core area of 1.6 mm² in TCFA collected from coronary arteries of patients who

died due to either cardiovascular or non-cardiovascular causes.¹⁶ Though these values vary slightly, they are similar in magnitude; more importantly, all three studies identified an unambiguous increase in necrotic core size from stable, fibrous lesions to the “vulnerable,” rupture-prone TCFA to ruptured plaques. A proposed explanation for larger necrotic cores portending worse outcomes posits that intrusion into the luminal space impedes coronary vasodilation and triggers downstream ischemia,²¹ and thus, fatal and non-fatal MI, regardless of clinical variables or degree of stenosis. Additionally, the necrotic core integrates upstream events (e.g., macrophage infiltration) that contribute to destabilization of the lesion and increased risk of rupture. Macrophages initially recruited from the bloodstream to scavenge harmful accumulation of lipids express matrix metalloproteinases that degrade collagen and decrease the mechanical stability of the lesion.²² In the present study, we have shown that elevated impedance accompanies larger necrotic cores. Necrotic cores develop from ingestion of accumulated lipids in the neointimal layer by infiltrating macrophages. The poor electrical conductivity of lipids and the low water content of fatty tissue contribute to the higher impedance of lipid-laden plaques. Furthermore, our histological results demonstrating that plaques with necrotic cores ≥ 1.75 mm² possessed concomitant stenosis of $\geq 50\%$ are in agreement with previous studies that revealed that a vast majority of plaque ruptures (for which large necrotic cores are a high-risk factor) occurred in vessels with $\geq 50\%$ luminal narrowing.²³

Conversely, a thinner fibrous cap has been demonstrated to indicate higher risk of rupture and thus adverse future events.^{18,20} The fibrous cap consists of a matrix rich in collagen and elastin²² and represents the “final line of defense” against thrombus formation by isolating thrombogenic necrotic cores from circulating coagulation factors. As producers of the fibrous matrix, SMCs play a stabilizing role in maintaining the fibrous cap, while infiltrating macrophages destabilize the cap via secretions of proteolytic enzymes, such as matrix metalloproteinases, thus leading degradation of the fibrous cap.²² The thinnest section along the fibrous cap is the most susceptible to mechanical disruption leading to rupture; the risk increases with decreasing cap thickness.²² In their histological assessment of coronary lesions from victims of sudden coronary death, Virmani et al. discovered that 95% of ruptured fibrous caps were thinner than 65 μ m.¹⁸ These findings led to the introduction of the term “thin-cap fibroatheromas,” which represent plaques at high risk of rupture. For plaques that do not undergo stabilization, the fibrous cap becomes or remains thin as the necrotic core continues to enlarge.²² Accordingly, plaques with thin fibrous caps capture upstream processes including necrotic core enlargement

that ultimately lead to a rupture-prone phenotype. In the present study, we note a higher impedance in plaques with thin fibrous caps. Our histological analyses revealed that the vast majority of large necrotic cores were accompanied by thin fibrous caps. We posit that the similar performance of EIS to detect large necrotic cores and thin fibrous caps is primarily driven by the necrotic core area.

In addition to compositional plaque characteristics, EIS, via phase delay, also illuminates plaque morphology through discrimination of arteries harboring luminal narrowing $\geq 70\%$. We observed a decrease in phase delay magnitude (phase delay is less negative, i.e., closer to zero) as stenosis severity increased. This trend possibly results from the reduced electrical capacitance that accompanies thicker artery layers (e.g., a thicker neointimal layer). Biological tissues exhibit both resistive and capacitive characteristics, the latter arising from cell membranes, which act as very thin capacitors. A purely capacitive system exhibits a phase delay magnitude of 90° , while a purely resistive system exhibits no phase delay (i.e., phase delay of 0°). With a thicker neointimal layer, there are more cells in series with each other. As capacitors are placed in series, the total capacitance of the system decreases. Consequently, the resistive behavior of the system becomes more prominent, and the phase delay approaches 0° . For acellular regions such as fibrotic tissue or necrotic cores, the decrease in phase delay magnitude may be attributed primarily instead to the increase in resistive behavior due to higher lipid content and/or lower water content, as seen in necrotic cores or fibrotic tissue. We emphasize, however, that the main proposed utility of EIS in CAD evaluation is not the determination of stenosis severity but the detection of rupture-prone lesions.

Intravascular ultrasound (IVUS) is a well-established, catheter-based imaging method capable of assessing vessel morphology and plaque burden. Limitations of IVUS, namely, relatively low spatial resolution and discrimination between plaque components,²⁴ may be overcome via pairing with complementary imaging modalities such as optical coherence tomography (OCT), near-infrared spectroscopy (NIRS), and near-infrared fluorescence (NIRF). The excellent spatial resolution of OCT permits detailed assessment of plaque characteristics, for example, in vivo measurement of fibrous cap thickness. NIRS detects and quantifies plaque lipid burden, an indicator for early disease progression that may be missed during angiography.²⁵ NIRF boasts deep tissue penetration and can assess plaque inflammation in vivo.²⁴ However, these modalities contend with their own limitations. OCT has limited tissue penetration; NIRS provides semiquantitative lipid content measurement; NIRF requires administration of a

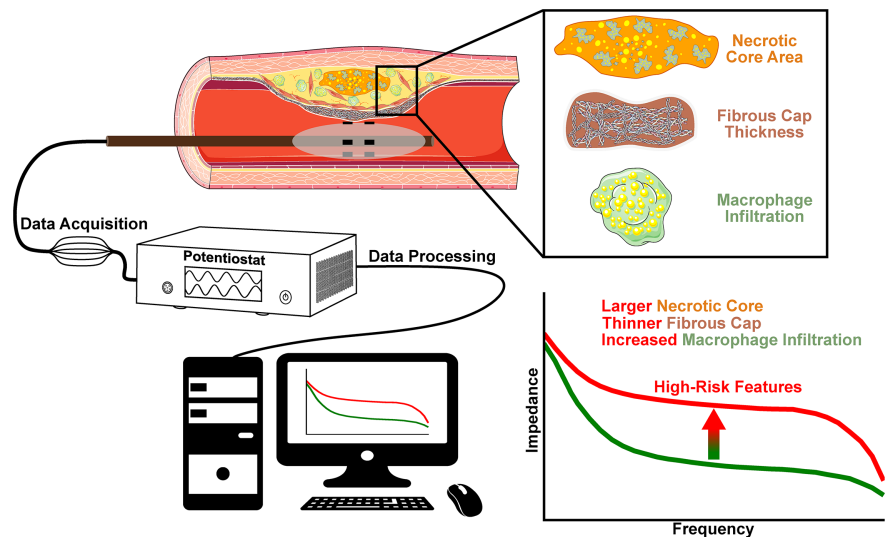
targeting probe and thus is subject to limitations inherent to a probe and its biodistribution.

Matrix metalloproteinases (MMPs) are important contributors to atherosclerotic plaque progression and destabilization.²⁶ MMPs, such as MMP-9, compromise the mechanical integrity of plaques through the degradation of collagen, the main structural component of plaques, particularly the fibrous cap.²⁷ MMP-9 can be activated by other MMPs (e.g., MMP-2, -3, -7, -13),^{26,28} proteolytic enzymes like tissue-type plasminogen activator or plasmin,²⁸ or environmental conditions such as low pH. MMP-9 may contribute to plaque progression beyond mechanical degradation. MMP-9 releases vascular endothelial growth factor (VEGF) from proteoglycans in the ECM, thus increasing VEGF bioavailability and impacting plaque neovascularization, a known risk factor of plaque instability. MMP-9 is also a key modulator of SMC migration into and proliferation within plaques. Studies in MMP-9^{-/-} mice demonstrated reduced SMC migration to the neointima and reduced neointima size²⁹ as well as impaired SMC adhesion to gelatin.³⁰ MMP-9 also functions in conjunction with plasminogen to regulate macrophage migration into atherosclerotic plaque.³¹

Lipoprotein-associated phospholipase A₂ (Lp-PLA₂) contributes to atherosclerotic plaque progression through the cleavage of phospholipids into oxidized non-esterified fatty acids (OxNEFA) and lysophospholipids.³² Lp-PLA₂ is secreted mainly by macrophages and circulates in a complex primarily with LDL, though Lp-PLA₂ may also complex with HDL.³³ Production of OxNEFA and lysophospholipids promote the expression of adhesion molecules, stimulate pro-inflammatory cytokines, and attracts inflammatory cells (e.g., macrophages) to the intima.^{32,34} These effects fuel a positive feedback loop in which recruited macrophages produce even more Lp-PLA₂. Accumulation of macrophages, foam cells, and cleaved phospholipids accelerates the development of a necrotic core and hence plaque progression. Histopathological studies reveal a concentration of Lp-PLA₂ in TCFAs and ruptured plaques^{35,36} and have established its association with rupture-prone plaque.^{36,37} Indeed, Lp-PLA₂ has been demonstrated across multiple studies to be a cardiovascular risk marker independent of traditional risk factors.^{38–40}

In the present translational study, we demonstrate the ability of invasive EIS sensors to unravel key atherosclerotic features that portend future rupture and adverse events in human CAD (Figure 6). We posit that EIS can serve as a complementary modality to invasive coronary angiography (ICA) for CAD evaluation. ICA detects plaque burden and distribution and may guide the EIS sensors to the proper location for plaque interrogation. Precise positioning of our EIS sensors under balloon deflation to the arterial segment of interest is

FIGURE 6 Electrochemical impedance spectroscopy characterization of high-risk coronary atherosclerotic features in humans. Summary schematic of EIS catheter deployment, signal acquisition, and data processing, with depiction of impedance profile changes leading to detection of high-risk coronary atherosclerotic features. EIS, electrochemical impedance spectroscopy.



guided during fluoroscopy via radiopaque markers positioned immediately distal and proximal to the balloon. Discrimination of necrotic core size, fibrous cap thickness, macrophage infiltration, and stenosis severity peaks within the frequencies of the “plateau region” and requires three to four seconds, including the time required for balloon inflation. EIS sensors may be integrated with a hollow-tube catheter design that permits continuous blood flow even during balloon inflation, thus obviating potential ischemia. Analysis of EIS measurements can be performed in real-time, thus reducing the delay between vessel interrogation and decision-making. We demonstrate that EIS sensors identify lesions harboring high-risk plaque features. EIS also provides the additional benefit of a secondary layer of stenosis assessment that may supplement visual estimation of luminal narrowing, known to be prone to variation. We propose a “threshold impedance” of 9 k Ω to identify high-risk plaque features, namely, large necrotic core ≥ 1.75 mm², thin fibrous cap ≤ 65 μ m, and ≥ 20 macrophages per HPF. The coupling of EIS with ICA may reveal rupture-prone lesions and could be integrated into subsequent decision-making toward the appropriate treatments and/or procedures.

4.1 | Limitations

Our study has limitations. This was a single-center study derived, however, from valuable and relatively rare human cardiac explants. Moreover, the diversity of interrogated arteries ranging from mild to moderate to severe coronary disease allowed for a comprehensive scrutiny of a wide range of atherosclerotic disease severity. Patients with ACS or a recent ACS event were not the target population for the present study.

Furthermore, EIS characterization of atherosclerotic plaques in these cardiac explants is not entirely representative of in vivo conditions. However, our group previously established the excellent correlation of ex vivo and in vivo EIS signals in an animal model of atherosclerosis and demonstrated the feasibility of in vivo EIS measurements without complications.^{11,13} Follow-up studies are needed for direct comparison of EIS with previously established intravascular methods for plaque characterization in humans. Additionally, plaque macrophage content was quantified using PU.1 as a histological marker. Although PU.1 is highly expressed in macrophages, other leukocytes such as B lymphocytes exhibit low levels of PU.1. However, given the large abundance of macrophages relative to B lymphocytes in atherosclerotic plaque, we do not anticipate that expression of PU.1 by non-macrophage leukocytes significantly impacts our analyses.

Future studies should assess the predictive ability of EIS to identify potential culprit lesions in vivo in human CAD prior to downstream events, as well as the utility of EIS in gauging atherosclerosis progression/stabilization in serial studies.

5 | CONCLUSION

EIS represents an invasive strategy for CAD evaluation in humans that identifies rupture-prone plaques. The combination of ICA with complementary EIS may help guide clinical decision-making toward the appropriate treatments and interventions.

AUTHOR CONTRIBUTIONS

M.C. and R.R.S.P. conceptualized the study. M.C., K.S., Y.S., Y.L., P.B., M.C.F., R.R.S.P. carried out the

investigation. M.C., K.S., and M.C.F. analyzed the data. M.C. prepared figures. M.C. and R.R.S.P. interpreted the results of experiments and prepared and wrote the original draft of the manuscript. M.C., K.S., Y.S., Y.L., P.B., M.C.F., R.R.S.P. reviewed and edited the manuscript and approved the final version of the manuscript. R.R.S.P. acquired funding.

ACKNOWLEDGEMENTS

None.

FUNDING INFORMATION

Dr. Packard is supported by VA Merit BX004558, NIH R56HL158569, and UCLA Cardiovascular Discovery Fund/Lauren B. Leichtman and Arthur E. Levine Investigator Award.

DISCLOSURES

The authors declare no competing interests.

DATA AVAILABILITY STATEMENT

Data underlying the present study may be made available upon reasonable request to the corresponding author.

ORCID

Michael Chen  <https://orcid.org/0000-0003-0694-6641>

Krit Suwannaphoom  <https://orcid.org/0009-0009-6036-829X>

Yas Sanaiha  <https://orcid.org/0000-0002-3976-5620>

Yuan Luo  <https://orcid.org/0000-0003-3153-7495>

Peyman Benharash  <https://orcid.org/0000-0002-4705-0262>

Michael C. Fishbein  <https://orcid.org/0000-0002-6591-6306>

René R. Sevag Packard  <https://orcid.org/0000-0002-8520-5843>

REFERENCES

- Martin SS, Aday AW, Almarzooq ZI, et al. 2024 heart disease and stroke statistics: a report of US and global data from the American Heart Association. *Circulation*. 2024;149:e347-e913.
- Gulati M, Levy PD, Mukherjee D, et al. 2021 AHA/ACC/AASE/CHEST/SAEM/SCCT/SCMR guideline for the evaluation and diagnosis of CHEST pain: a report of the American College of Cardiology/American Heart Association joint committee on clinical practice guidelines. *Circulation*. 2021;144:e368-e454.
- Tomaniak M, Katagiri Y, Modolo R, et al. Vulnerable plaques and patients: state-of-the-art. *Eur Heart J*. 2020;41:2997-3004.
- Gaba P, Gersh BJ, Muller J, Narula J, Stone GW. Evolving concepts of the vulnerable atherosclerotic plaque and the vulnerable patient: implications for patient care and future research. *Nat Rev Cardiol*. 2023;20:181-196.
- Mushtaq S, De Araujo GP, Garcia-Garcia HM, et al. Long-term prognostic effect of coronary atherosclerotic burden. *Circ Cardiovasc Imaging*. 2015;8:e002332.
- Packard RRS, Li D, Budoff MJ, Karlsberg RP. Fractional flow reserve by computerized tomography and subsequent coronary revascularization. *Eur Heart J Cardiovasc Imaging*. 2017;18:145-152.
- Chen M, Almeida SO, Sayre JW, Karlsberg RP, Packard RRS. Distal-vessel fractional flow reserve by computed tomography to monitor epicardial coronary artery disease. *Eur Heart J Cardiovasc Imaging*. 2024;25:163-172.
- Packard RRS, Cooke CD, Van Train KF, et al. Development, diagnostic performance, and interobserver agreement of a ¹⁸F-flurpiridaz PET automated perfusion quantitation system. *J Nucl Cardiol*. 2022;29:698-708.
- Packard RRS, Votaw JR, Cooke CD, Van Train KF, Garcia EV, Maddahi J. ¹⁸F-flurpiridaz positron emission tomography segmental and territory myocardial blood flow metrics: incremental value beyond perfusion for coronary artery disease categorization. *Eur Heart J Cardiovasc Imaging*. 2022;23:1636-1644.
- Süselbeck T, Thielecke H, Köchlin J, et al. Intravascular electric impedance spectroscopy of atherosclerotic lesions using a new impedance catheter system. *Basic Res Cardiol*. 2005;100:446-452.
- Packard RRS, Zhang X, Luo Y, et al. Two-point stretchable electrode Array for Endoluminal electrochemical impedance spectroscopy measurements of lipid-laden atherosclerotic plaques. *Ann Biomed Eng*. 2016;44:2695-2706.
- Chen M, Neverova N, Xu S, et al. Invasive electrochemical impedance spectroscopy with phase delay for experimental atherosclerosis phenotyping. *FASEB J*. 2024;38:e23700.
- Packard RRS, Luo Y, Abiri P, et al. 3-D electrochemical impedance spectroscopy mapping of arteries to detect metabolically active but Angiographically invisible atherosclerotic lesions. *Theranostics*. 2017;7:2431-2442.
- Walsh JC, DeKoter RP, Lee H-J, et al. Cooperative and antagonistic interplay between PU.1 and GATA-2 in the specification of myeloid cell fates. *Immunity*. 2002;17:665-676.
- Chambers C, Cermakova K, Chan YS, et al. SWI/SNF blockade disrupts PU.1-directed enhancer programs in normal hematopoietic cells and acute myeloid leukemia. *Cancer Res*. 2023;83:983-996.
- Cheruvu PK, Finn AV, Gardner C, et al. Frequency and distribution of thin-cap fibroatheroma and ruptured plaques in human coronary arteries: a pathologic study. *J Am Coll Cardiol*. 2007;50:940-949.
- Kolodgie FD, Gold HK, Burke AP, et al. Intraplaque hemorrhage and progression of coronary atheroma. *N Engl J Med*. 2003;349:2316-2325.
- Virmani R, Kolodgie FD, Burke AP, Farb A, Schwartz SM. Lessons from sudden coronary death. *Arterioscler Thromb Vasc Biol*. 2000;20:1262-1275.
- Narula J, Garg P, Achenbach S, Motoyama S, Virmani R, Strauss HW. Arithmetic of vulnerable plaques for noninvasive imaging. *Nat Rev Cardiol*. 2008;5:S2-S10.
- Burke AP, Farb A, Malcom GT, Liang Y, Smialek J, Virmani R. Coronary risk factors and plaque morphology in men with coronary disease who died suddenly. *N Engl J Med*. 1997;336:1276-1282.

21. Ahmadi A, Stone GW, Leipsic J, et al. Association of coronary stenosis and plaque morphology with fractional flow reserve and outcomes. *JAMA Cardiol.* 2016;1:350-357.
22. Bentzon JF, Otsuka F, Virmani R, Falk E. Mechanisms of plaque formation and rupture. *Circ Res.* 2014;114:1852-1866.
23. Fishbein MC, Siegel RJ. How big are coronary atherosclerotic plaques that rupture? *Circulation.* 1996;94:2662-2666.
24. Khraishah H, Jaffer FA. Intravascular molecular imaging: near-infrared fluorescence as a new frontier. *Front Cardiovasc Med.* 2020;7:587100.
25. Kilic ID, Caiazzo G, Fabris E, et al. Near-infrared spectroscopy-intravascular ultrasound: scientific basis and clinical applications. *Eur Heart J Cardiovasc Imaging.* 2015;16:1299-1306.
26. Dollery CM, Libby P. Atherosclerosis and proteinase activation. *Cardiovasc Res.* 2006;69:625-635.
27. Loftus IM, Naylor AR, Goodall S, et al. Increased matrix metalloproteinase-9 activity in unstable carotid plaques. *Stroke.* 2000;31:40-47.
28. Yabluchanskiy A, Ma Y, Iyer RP, Hall ME, Lindsey ML. Matrix metalloproteinase-9: many shades of function in cardiovascular disease. *Phys Ther.* 2013;28:391-403.
29. Cho A, Reidy MA. Matrix metalloproteinase-9 is necessary for the regulation of smooth muscle cell replication and migration after arterial injury. *Circ Res.* 2002;91:845-851.
30. Johnson C, Galis ZS. Matrix metalloproteinase-2 and -9 differentially regulate smooth muscle cell migration and cell-mediated collagen organization. *Arterioscler Thromb Vasc Biol.* 2004;24:54-60.
31. Gong Y, Hart E, Shchurin A, Hoover-Plow J. Inflammatory macrophage migration requires MMP-9 activation by plasminogen in mice. *J Clin Invest.* 2008;118:3012-3024.
32. Rosenson RS, Hurt-Camejo E. Phospholipase A2 enzymes and the risk of atherosclerosis. *Eur Heart J.* 2012;33:2899-2909.
33. Rosenson RS, Stafforini DM. Modulation of oxidative stress, inflammation, and atherosclerosis by lipoprotein-associated phospholipase A2. *J Lipid Res.* 2012;53:1767-1782.
34. Silva IT, Mello AP, Damasceno NR. Antioxidant and inflammatory aspects of lipoprotein-associated phospholipase A2 (Lp-PLA2): a review. *Lipids Health Dis.* 2011;10:1-10.
35. Münzel T, Gori T. Lipoprotein-associated phospholipase A2, a marker of vascular inflammation and systemic vulnerability. *Eur Heart J.* 2009;30:2829-2831.
36. Kolodgie FD, Burke AP, Skorija KS, et al. Lipoprotein-associated phospholipase A2 protein expression in the natural progression of human coronary atherosclerosis. *Arterioscler Thromb Vasc Biol.* 2006;26:2523-2529.
37. Lavi S, McConnell JP, Rihal CS, et al. Local production of lipoprotein-associated phospholipase A2 and lysophosphatidylcholine in the coronary circulation. *Circulation.* 2007;115:2715-2721.
38. Packard CJ, O'Reilly DSJ, Caslake MJ, et al. Lipoprotein-associated phospholipase A2 as an independent predictor of coronary heart disease. *N Engl J Med.* 2000;343:1148-1155.
39. Ballantyne CM, Hoogeveen RC, Bang H, et al. Lipoprotein-associated phospholipase A2, high-sensitivity C-reactive protein, and risk for incident coronary heart disease in middle-aged men and women in the atherosclerosis risk in communities (ARIC) study. *Circulation.* 2004;109:837-842.
40. Koenig W, Khuseynova N, Löwel H, Trischler G, Meisinger C. Lipoprotein-associated phospholipase A2 adds to risk prediction of incident coronary events by C-reactive protein in apparently healthy middle-aged men from the general population. *Circulation.* 2004;110:1903-1908.

SUPPORTING INFORMATION

Additional supporting information can be found online in the Supporting Information section at the end of this article.

How to cite this article: Chen M, Suwannaphoom K, Sanaiha Y, et al. Electrochemical impedance spectroscopy unmasks high-risk atherosclerotic features in human coronary artery disease. *The FASEB Journal.* 2024;38:e70069. doi:[10.1096/fj.202401200R](https://doi.org/10.1096/fj.202401200R)